CHEMISTRY OF MATERIALS
Article

Chem. Mater. **2009,** *21,* 3337–3345 3337
DOI:10.1021/cm900875s

$Ce_{1-x}Ru_xO_{2-\delta}$ ($x = 0.05, 0.10$): A New High Oxygen Storage Material and Pt, Pd-Free Three-Way Catalyst

Preetam Singh and M. S. Hegde*

Solid State and Structural Chemistry Unit, Indian Institute of Science, Bangalore, 560012, India

Received March 30, 2009. Revised Manuscript Received May 11, 2009

Nanocrystalline $Ce_{1-x}Ru_xO_{2-\delta}$ ($x = 0.05$ and 0.10) of 8−10 nm sizes have been synthesized by hydrothermal method using melamine as complexing agent. Compounds have been characterized by powder X-ray diffraction (XRD), transmission electron microscopy (TEM), X-ray photoelectron spectroscopy (XPS), and energy-dispersive X-ray analysis (EDX) and their structures have been refined by the Rietveld method. The compounds crystallize in fluorite structure and the composition is $Ce_{1-x}Ru_xO_{2-x/2}$ where Ru is in +4 state and Ce is in mixed-valence (+3, +4) state. Substitution of Ru^{4+} ion in CeO_2 activated the lattice oxygen. $Ce_{1-x}Ru_xO_{2-x/2}$ reversibly releases 0.22[O] and 0.42[O] for $x = 0.05$ and 0.10, respectively, which is higher than the maximum possible OSC of 0.22 [O] observed for $Ce_{0.50}Zr_{0.50}O_2$. Utilization of Higher OSC of $Ce_{1-x}Ru_xO_{2-\delta}$ ($x = 0.05$ and 0.10) is also reflected in terms of low-temperature CO oxidation with these catalysts, both in the presence and absence of feed oxygen. The Ru^{4+} ion acts as an active center for reducing molecules (CO, hydrocarbon "HC") and oxide ion vacancy acts as an active center for O_2 and NO, leading to low-temperature NO conversion to N_2. Thus due to Ru^{4+} ion, $Ce_{1-x}Ru_xO_{2-\delta}$ is not just a high oxygen storage material but also shows high activity toward CO, hydrocarbon "HC" oxidation, and NO reduction by CO at low temperature with high N_2 selectivity for three-way catalysis.

1. Introduction

The amount of lattice oxygen that can be reversibly exchanged from CeO_2 is called oxygen storage capacity (OSC).[1,2]

$$CeO_2 + \delta CO/H_2 \rightarrow CeO_{2-\delta} + \delta CO_2/H_2O \quad (1)$$

$$CeO_{2-\delta} + \delta/2O_2 \rightarrow CeO_2 \quad (2)$$

Because of its OSC, ceria has attracted a great deal of attention in autoexhaust catalysis, fuel cells, solar cells, etc.[3−5] The extent of reducibility of CeO_2 or OSC (δ) is dependent on the size of crystallites: the smaller the crystallite size, the higher the OSC.[6] Oxygen storage capacity and catalytic performance of ceria in autoexhaust catalysis can be enhanced by isovalent and aliovalant metal ion substitution in CeO_2, as in $Ce_{1-x}Zr_xO_2$,[7−10] $Ce_{1-x}Ti_xO_2$,[11,12] $Ce_{1-x}Fe_xO_{2-x/2}$,[6] $Ce_{1-x}Cr_xO_{2+\delta}$.[13] OSC at lower temperature in nanocrystalline $Ce_{0.5}Zr_{0.5}O_2$ is attributed to cation ordering.[10] Higher OSC of these substituted CeO_2 retaining fluorite structure is traced to destabilization of oxygen sublattice in the fluorite structure leading to long and short M−O bonds compared to Ce−O bond in CeO_2.[14,15] The longer M−O bonds being weaker, they can easily react with CO or hydrocarbon "HC". Only under fuel-rich conditions is lattice oxygen utilized to form CO_2 or H_2O from unburnt CO and "HC". However, under stoichiometric combustion conditions, CO, "HC", and NO*x* absorbed on the noble metal atoms react with each other or with O_2, forming CO_2, H_2O, and N_2 and thus abating pollutant from exhaust. Thus multicomponent catalyst with noble metals Pt, Pd, Rh impregnated on silica or Al_2O_3 along with OSC materials forms a

*Corresponding author. Email : mshegde@sscu.iisc.ernet.in. Phone: 91-80-2293 2614. Fax: 91-80-2360 1310.

(1) Yao, H. C., Yao Yu Y. F. **1984**, *86*, 254.
(2) Trovareli, A. *Catal. Rev. Sci. Eng*. **1996**, *38*, 439.
(3) Murray, E. P.; Tsai, T.; Barnett, S. A. *Nature* **1999**, *400*, 649.
(4) Fu, Q.; Saltsbarg, H.; Flytzani-Stephanopoulos, M. *Science* **2003**, *301*, 935.
(5) Corma, A.; Atienzar, P.; Gracia, H.; Chane-Ching, J. Y. *Nat. Mater*. **2004**, *3*, 394.
(6) Singh, P.; Hegde, M. S. *J. Solid State Chem*. **2008**, *181*, 3248.
(7) Fornasiero, P.; Di Monte, R.; Ranga Rao, G.; Kăspar, J; Meriani, S.; Trovarelli, A.; Graziani, M. *J. Catal*. **1995**, *151*, 168.
(8) Di Monte, R.; Kašpar, J. *J. Mater. Chem*. **2005**, *15*, 633.
(9) Baidya, T.; Hegde, M. S.; Gopalakrishnan, J. *J. Phys. Chem. B* **2007**, *111*, 5149.
(10) Alessandri, I.; Banares, M. A.; Depero, L. E.; Ferroni, M.; Fornasiero, P.; Gennari, F. C.; Hickey-Martinez, M. V.; Montini, T. *Top. Catal*. **2006**, *41*, 35.
(11) Baidya, T.; Dutta, G.; Hegde, M. S.; Waghmare, U. V. *Dalton Trans*. **2009**, 455.
(12) Baidya, T.; Marimuthu, A.; Hegde, M. S.; Ravishankar, N.; Madras, G. *J. Phys. Chem. C* **2007**, *111*, 830.
(13) Singh, P.; Hegde, M. S.; Gopalakrishnan, J. *Chem. Mater*. **2008**, *20*, 7268.
(14) Nagai, Y.; Yamamoto, T.; Tanaka, T.; Yoshida, S.; Nonaka, T.; Okamoto, T; Suda, A.; Sugiura, M. *Catal. Today* **2002**, *74*, 225.
(15) Dutta, G.; Waghmare, U. V.; Baidya, T.; Hegde, M. S.; Priolkar, K. R.; Sarode, P. R. *Catal. Lett*. **2006**, *108*, 165.

Published on Web 06/04/2009

complete auto exhaust catalyst.[16−19] In recent years, we have shown noble metal ionic catalyst where noble metals in the form of ion are substituted in CeO_2 and they have shown higher catalytic activity in exhaust catalysis than the corresponding metals supported on silica or Al_2O_3.[20−25]

Can we design a uniform solid catalyst that acts as an OSC material and also contain adsorption sites for CO, "HC" and NO_x? With this idea, we have synthesized nanocrystalline $Ce_{1-x}Ru_xO_{2-\delta}$ ($x = 0.05$, 0.10) where Ru ion substitution can enhance the OSC and the Ru ions can act as absorption sites for reductant molecule. In this paper we report the synthesis, structure, and catalytic properties of Ru ion substituted CeO_2 viz, $Ce_{1-x}Ru_xO_{2-x/2}$ ($x = 0.05$ and 0.10). $Ce_{1-x}Ru_xO_{2-x/2}$ nanocrystallites of 8−10 nm sizes are synthesized by hydrothermal method using melamine as a complexing agent. With 10% Ru^{4+} ion substitution in CeO_2, OSC is higher than $Ce_{0.5}Zr_{0.5}O_2$ at much lower temperature. $Ce_{1-x}Ru_xO_{2-x/2}$ has shown high catalytic for CO and "HC" oxidation and NO*x* reduction avoiding the use of Pt, Pd metals.

2. Experimental Section

$Ce_{1-x}Ru_xO_{2-\delta}$ solid solutions were synthesized by the hydrothermal method from the starting materials, $(NH_4)_2Ce(NO_3)_6$ (CAN), $RuCl_3 \cdot xH_2O$, and melamine by taking them in a $1-x:x:2$ molar ratio. For the synthesis of $Ce_{0.95}Ru_{0.05}O_{2-\delta}$, 2.375 mM ceric ammonium nitrate, $Ce(NH_4)_2(NO_3)_6$ (CAN), is dissolved in 20 mL of distilled water and 0.135 mM $RuCl_3 \cdot xH_2O$(Aldrich) is dissolved in 5 mL of water and both the solutions were mixed in 5.0 mM melamine ($C_3N_6H_6$) solution made in hot water (75 °C). There is no change in the orange color of CAN + $RuCl_3 \cdot xH_2O$ solution when melamine added. The solution turned into a gel. The resulting gel was stirred for 10 min in warm condition. The gel was transferred to three autoclave bombs of 20 mL capacity with 75% of filling and they were placed in a hot air oven at 200 °C for 24 h. The precipitated black colored solid was filtered and dried in a hot air oven at 120 °C for 6 h.

X-ray diffraction patterns of powders were recorded in a Phillips X'Pert diffractometer using Cu Kα radiation at scan rate of 0.25° min^{-1} with a 0.01° step size in the 2θ range between 10 and 80°. Cu K_β radiation was filtered with a graphite crystal post monochromator. Structures were refined by the Rietveld method, using the FullProf-fp2k program.[26]

For transmission electron microscopy (TEM), a toluene dispersion of the sample was dropped onto the holey carbon-coated Cu grids and images were recorded with FEI Technai 20 at 200 kV. XPS of selected samples were recorded in a Thermo Scientific Multilab 2000 instrument. Binding energies reported here are with reference to C (1s) at 284.5 eV and they are accurate within ± 0.1 eV.

To study the redox properties of $Ce_{1-x}Ru_xO_{2-\delta}$, hydrogen uptake measurements were performed in a micro reactor of length 30 and 0.4 cm internal diameter with 5.49% H_2/Ar (certified calibration gas mixture from Bhoruka gases Ltd., India) flowing at 30 sccm at a linear heating rate of 10 °C min^{-1} up to 500 °C. Volume of hydrogen uptake was calibrated against CuO. CO oxidation, Hydrocarbon oxidation and NO reduction by CO were performed in a micro reactor of length 30 and 0.4 cm internal diameter with total flow 100 sccm of reactant gases over 200 mg of catalyst at a linear heating rate of 10 °C min^{-1} up to 500 °C. CO oxidation over the catalysts are carried out with 200 mg of each catalyst at a space velocity of 43 000 CC h^{-1} with 1:1 vol % CO and O_2 with a linear heating rate of 10 °C min^{-1}. Hydrocarbon (HC) oxidation over the $Ce_{1-x}Ru_xO_{2-x/2}$ ($x = 0.05$ and 0.10) oxides are carried out with a mixture having the composition 470 ppm of both propene and propane, 870 ppm of both ethylene and acetylene, 124 000 ppm of CO_2, and a stoichiometric amount (10 000 ppm) of O_2. Total gas flow has been kept 100 CC/min over 200 mg of catalysts. NO reduction by CO over the catalysts are carried out with 200 mg of each catalyst at space velocity of 43 000 CC h^{-1} with 0.5:0.5 vol % CO and NO with a linear heating rate of 3 °C min^{-1}. Gaseous products were analyzed by means of a quadrupole mass spectrometer and online gas chromatograph.

3. Results and Discussion

Ru ion substituted CeO_2 could not be precipitated in hydrothermal bombs with CAN + $RuCl_3$ solution only and with NH_3, NaOH, and diethylenetriamine; RuO_2 was separated out with CeO_2 in each of these experiments. Only with melamine as the complexing agent was black colored $Ce_{1-x}Ru_xO_{2-\delta}$ precipitated, and the yield was quantitative. The powder X-ray diffraction patterns of as prepared CeO_2 and $Ce_{1-x}Ru_xO_{2-\delta}$ for the composition ($x = 0.05$, 0.1 and 0.15) with melamine at 200 °C are shown in Figure 1a−d. The X-ray diffraction pattern of $Ce_{1-x}Ru_xO_{2-\delta}$ ($0 \le x \le 0.10$) is indexed to fluorite structure and diffraction lines because the Ce−melamine complex, Ru−melamine complex, RuO_2, and Ru metal are not observed. When compound is made with $x = 0.15$ Ru, RuO_2, and Ru metal impurity peaks are observed in powder XRD pattern (Figure 1d). Thus only up to 10% Ru ion can be substituted for Ce^{4+} in ceria by this method. Melamine is a weak complexing agent because of its planar benzene like structure and mild basic character (pH ∼8). It forms a weak complex by its $-NH_2$ lone pair with both the metal ions, which can be broken under hydrothermal conditions. Because of simultaneous and slow hydrolysis of Ce and Ru complexes at relatively low pH, $Ce_{1-x}Ru_xO_{2-\delta}$ ($0 \le x \le 0.10$) nanocrystallites are precipitated. The Rietveld refined XRD profiles of $Ce_{0.95}Ru_{0.05}O_{2-\delta}$ and $Ce_{0.90}Ru_{0.10}O_{2-\delta}$ are shown in panels a

(16) Cant, N. W.; Hicks, P. C.; Lenon, B. S. *J. Catal.* **1978**, *54*, 372.
(17) Kummer, J. T *J. Phys. Chem.* **1986**, *90*, 4747.
(18) Pérez-Hernández, R.; Aguilar, F.; Gómez-Cortés, A.; Díaz, G. *Catal. Today* **2005**, *107−108*, 175.
(19) Guo, Y.; Lu, G.; Zhang, Z.; Zhang, S; Qi, y.; Liu, Y. *Catal. Today* **2007**, *126*, 296.
(20) Bera, P.; Patil, K. C.; Jayaram, V.; Subbanna, G. N.; Hegde, M. S. *J. Catal.* **2000**, *196*, 293.
(21) Roy, S.; Mari Muthu, A.; Hegde, M. S.; Madras, G. *Appl. Catal. B: Environ.* **2007**, *71*, 23.
(22) Bera, P.; Aruna, S. T.; Hegde, M. S. *Chem. Mater.* **2002**, *14*, 3591.
(23) Bera, P.; Priolkar, K. R.; Gayen, A.; Sarode, P. R.; Hegde, M. S.; Emura, S.; Kumashiro, R.; Jayaram, V.; Subbanna, G. N. *Chem. Mater.* **2003**, *15*, 2049.
(24) Priolkar, K. R.; Bera, P.; Sarode, P. R.; Hegde, M. S.; Emura, S.; Kumashiro, R.; Lalla, N. P. *Chem. Mater.* **2002**, *14*, 2120–2128.
(25) Bera, P.; Patil, K. C.; Hegde, M. S. *Phys. Chem. Chem. Phys.* **2000**, *2*, 3715.
(26) Rodriguez-Carvajal, J. Multipattern Rietveld Refinment Program Fullprof 2k, version 3.30; Institut Laue-Langevin: Grenoble, France, 2005.

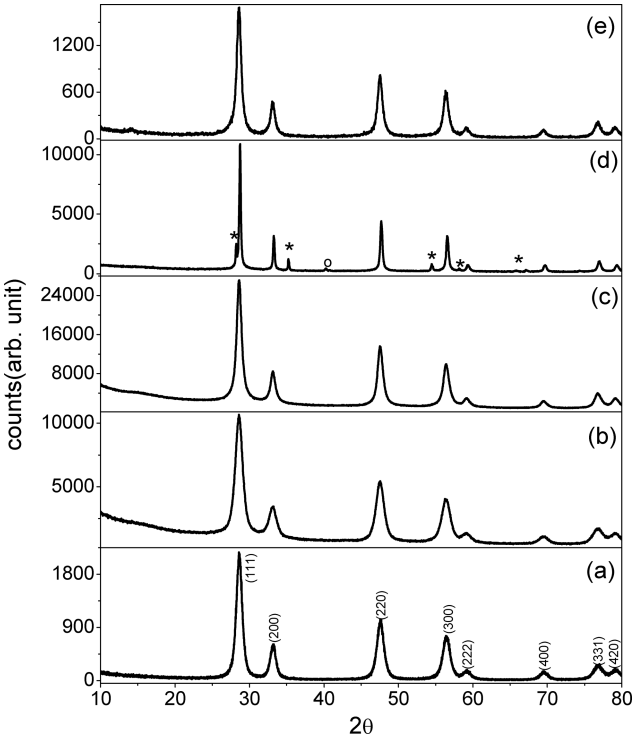

Figure 1. Powder XRD pattern of as prepared (a) CeO_2, (b) $Ce_{0.95}Ru_{0.05}O_{2-\delta}$, (c) $Ce_{0.90}Ru_{0.10}O_{2-\delta}$, (d) $Ce_{0.85}Ru_{0.15}O_{2-\delta}$ (* denotes peaks corresponding to RuO_2 and ○ corresponds to Ru metal), and (e) $Ce_{0.90}Ru_{0.10}O_{2-\delta}$ reduced in H_2 up to 500 °C.

and b in Figure 2, respectively. The refined X-ray profiles fitted well with the observed X-ray data. Crystallite sizes were estimated by following the Scherrer formula[27]

$$\text{crystallite size}(d) = 0.9\lambda/\beta\cos\theta \qquad (1)$$

where λ is the wavelength of X-ray, β is the full width at half maxima (fwhm) in radians, and θ is the diffraction angle. fwhm was estimated by the equation[28]

$$\beta = (U\tan^2\theta + V\tan\theta + W)^{1/2} \qquad (2)$$

By taking the U, V, and W values from the Rietveld refinement data for (111), (200), (220), and (311) diffraction lines, the crystallite sizes are found to be in the range of 8−0 nm. Crystallite size obtained for $Ce_{1-x}Ru_xO_{2-\delta}$ (x = 0.05 and 0.10) from powder XRD data along with lattice parameter, R_f, R_{bragg}, and χ^2 are summarized in Table 1. There is a slight increase in lattice parameter of $Ce_{1-x}Ru_xO_{2-\delta}$ with increasing Ru ion substitution in CeO_2. Composition is confirmed by EDX analysis.

Bright-field and HRTEM images of $Ce_{0.90}Ru_{0.10}O_{2-\delta}$ are shown in image a and b in Figure 3. Ring type diffraction pattern is indexed to fluorite structure given in the inset of Figure 3a. Average crystallites size of $Ce_{0.90}Ru_{0.10}O_{2-\delta}$ is 10 nm. Sizes obtained from TEM study agree well with XRD data. Crystallites due to RuO_2 or Ru metal have not been isolated in the HRTEM.

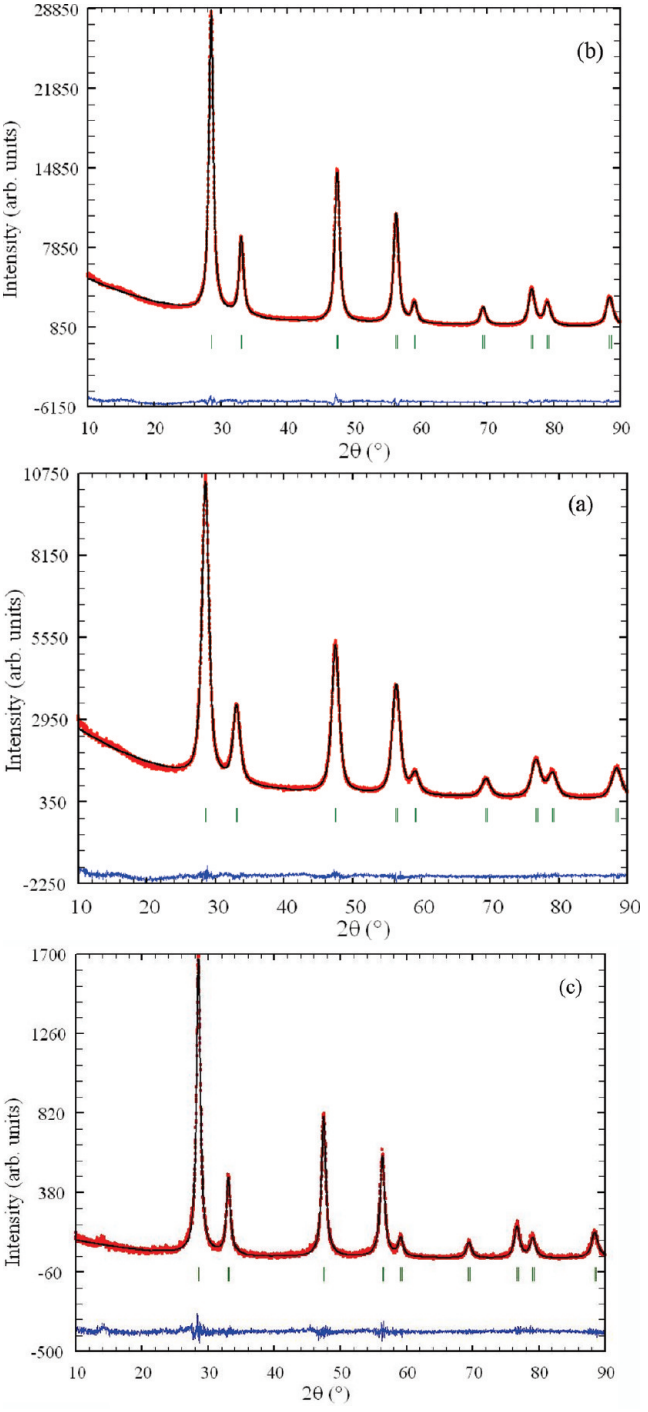

Figure 2. (a) Rietveld refined XRD profile of $Ce_{0.95}Ru_{0.05}O_{2-\delta}$, (b) Rietveld refined powder XRD pattern $Ce_{0.90}Ru_{0.10}O_{2-\delta}$, and (c) Rietveld refined powder XRD pattern of $Ce_{0.90}Ru_{0.10}O_{2-\delta}$ reduced in H_2 up to 500 °C.

The oxidation states of Ru and Ce in $Ce_{1-x}Ru_xO_{2-\delta}$ are analyzed by X-ray photoelectron spectroscopy (XPS). In XPS, Ru($3d_{5/2}$, $_{3/2}$) states are observed along with C(1s); therefore, the Ru(3p) region is also examined to assign the oxidation state of Ru ion. Core level Ru(3d) spectra in Ru metal and RuO_2 are given in spectra a and b in Figure 4 along with Ru(3d) spectra from $Ce_{0.95}Ru_{0.05}O_{2-\delta}$ and $Ce_{0.90}Ru_{0.10}O_{2-\delta}$ in panels c and d in Figure 4. Ru(3d) spectra is resolved in to C(1s), Ru($3d_{5/2}$), and Ru($3d_{3/2}$) states. In Ru metal and RuO_2,

(27) Cullity, B. D. Elements of X-ray Diffraction, 2nd ed.; Addison-Wesley: Reading, MA, 1978.
(28) Caglioti, G.; Paoletti, A.; Ricci, F. P. *Nucl. Instrum. Methods Phys. Res.* **1958**, *3*, 223.

Table 1. Structural parameter of $Ce_{1-x}Ru_xO_{2-x/2}$

compd	condition	lattice parameter	χ^2	R_B	R_f	avg crystallite sizes from Rietveld refinement (TEM) (nm)
CeO_2	as-prepared	5.4135 (4)	3.12	2.38	3.12	10.9 (10 ± 1)
$Ce_{0.95}Ru_{0.05}O_{1.97}$	as-prepared	5.4142 (1)	1.83	2.38	1.52	6.9
$Ce_{0.90}Ru_{0.10}O_{1.94}$	as-prepared	5.4149 (2)	3.70	2.36	1.75	10.7 (9 ± 2)
$Ce_{0.90}Ru_{0.10}O_{1.52}$	$Ce_{0.90}Ru_{0.10}O_{1.94}$ reduced in H_2 up to 500 °C	5.4154 (1)	1.18	2.13	1.40	10.9

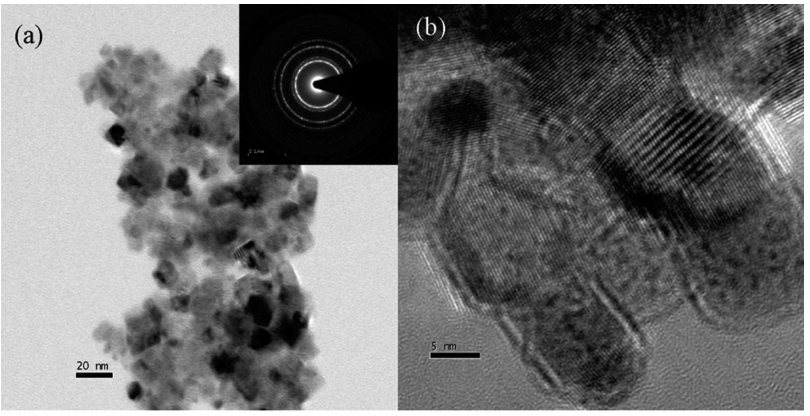

Figure 3. Bright-field and dark-field image and in inset electron diffraction pattern of $Ce_{0.90}Ru_{0.10}O_{2-\delta}$.

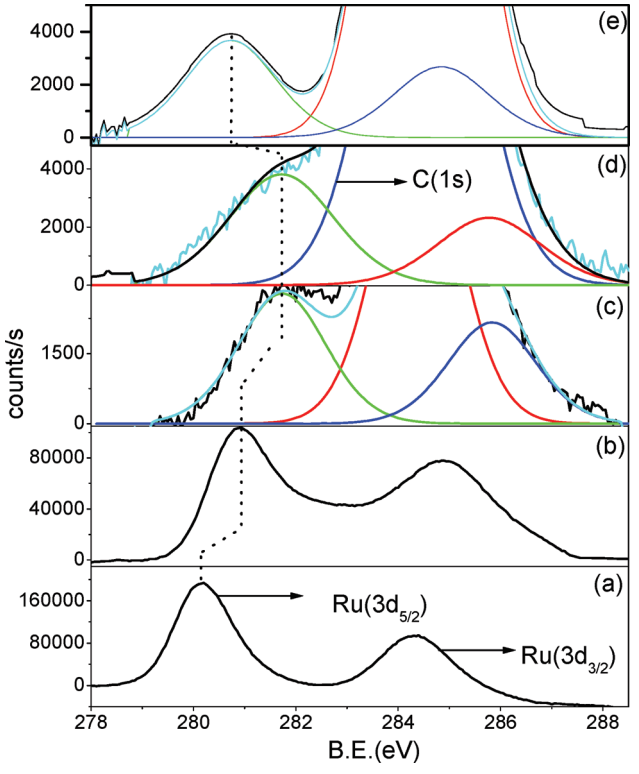

Figure 4. Ru (3d) core level XPS of (a) Ru metal, (b) RuO_2, (c) $Ce_{0.95}Ru_{0.05}O_{1.97}$, (d) $Ce_{0.90}Ru_{0.10}O_{1.94}$, and (d) H_2-reduced $Ce_{0.90}Ru_{0.10}O_{1.94}$.

$Ru(3d_{5/2})$ binding energies are observed at 280.1 and 280.7 eV, respectively. These values agree well with reported values.[29] The $Ru(3d_{5/2})$ peak in $Ce_{0.95}Ru_{0.05}O_{2-\delta}$ and $Ce_{0.90}Ru_{0.10}O_{2-\delta}$ is observed at 281.4 eV, which is higher than the $Ru(3d_{5/2})$ peak in RuO_2. The shift in binding energy values for Ru^0 in Ru metal to Ru^{4+} in RuO_2 is small because RuO_2 is a metallic oxide.[30] $Ru(3d_{5/2})$ is observed at 281.4 eV in $RuO_2 \cdot xH_2O$ and at 282.5 eV in RuO_3.[29,31] $Ru(3d_{5/2})$ binding energy at 281.4 eV in $Ce_{0.90}Ru_{0.10}O_{2-\delta}$ agrees well with the binding energy value for Ru^{4+} ion in $RuO_2 \cdot xH_2O$. Thus Ru is in the +4 state in $Ce_{1-x}Ru_xO_{2-\delta}$. Ru(3p) spectra for RuO_2 and Ru metal and $Ce_{0.90}Ru_{0.10}O_{2-\delta}$ are shown in spectra a to d in Figure 5. $Ru(3p_{3/2})$ is observed at 461.6 and 462.7 eV in Ru metal and RuO_2, respectively. In $Ce_{0.95}Ru_{0.05}O_{2-\delta}$ and $Ce_{0.90}Ru_{0.10}O_{2-\delta}$, the $Ru(3p_{3/2})$ peak is observed at 463.1 eV, which is also shifted to a higher value compared to RuO_2. Thus an XPS study of the Ru(3p) region also confirmed that Ru is in the +4 state in $Ce_{1-x}Ru_xO_{2-\delta}$ ($x = 0.05, 0.10$).

Core level XPS of Ce(3d) of as-prepared CeO_2, $Ce_{0.95}Ru_{0.05}O_{2-\delta}$, and $Ce_{0.90}Ru_{0.10}O_{2-\delta}$ are shown in Figure 6a−c, respectively. The Ce^{4+} $(3d_{5/2})$ peak observed at 882.7 eV along with satellite peaks at 6.4 and 16 eV below the main peak are characteristic of Ce^{4+} in CeO_2.[31] Ce^{3+}(3d) in Ce_2O_3 is characterized by $Ce(3d_{5/2})$ at 883.3 eV along with an intense satellite at 887.1 eV.[32] Thus, partial filling of the valley between $Ce^{4+}(3d_{5/2})$ at 882.7 eV and its satellite at 889.1 eV shows that Ce is in mixed valent (+4, +3) state in $Ce_{0.90}Ru_{0.10}O_{2-\delta}$. Ce(3d) spectrum was therefore resolved into Ce^{3+} and Ce^{4+} components in $Ce_{0.90}Ru_{0.10}O_{2-\delta}$; it is found that in $Ce_{0.90}Ru_{0.10}O_{2-\delta}$, around ∼12% of Ce is present as Ce^{3+} and the rest in Ce^{4+} state. Similarly, ∼6% of Ce^{3+} observed in $Ce_{0.95}Ru_{0.05}O_{2-\delta}$. Therefore amount of Ce^{3+} is close to amount of Ru present in $Ce_{1-x}Ru_xO_{2-\delta}$. Accordingly, formulas can be written as $Ce_{0.95}Ru_{0.05}O_{1.97}$

(29) Kim, K. S.; Winograd, N. *J. Catal.* **1974**, *35*, 66.
(30) Rogers, D. B.; Shannon, R. D.; Slight, A. W.; Gilson, J. L. *Inorg. Chem.* **1969**, *8*, 841.
(31) Sakurai, T.; Hinatsu, Y.; Takahashi, A.; Fujisawa, G. *J. Phys. Chem.* **1985**, *89*, 1892–1896.
(32) Kotani, A.; Ogasawara, H. *J. Electron Spectrosc. Relat. Phenom.* **1992**, *60*, 257.

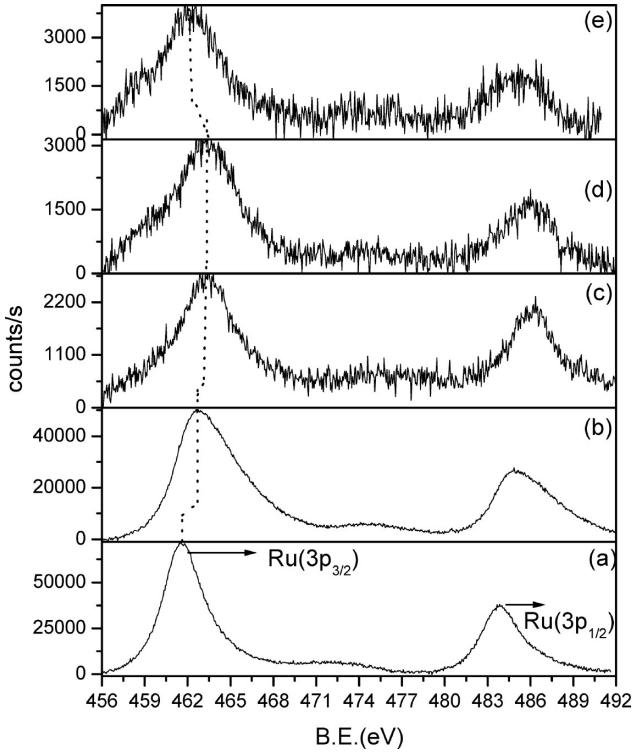

Figure 5. Ru (3p) core level XPS of (a) Ru metal, (b) RuO_2, (c) $Ce_{0.95}Ru_{0.05}O_{1.97}$, (d) $Ce_{0.90}Ru_{0.10}O_{1.94}$, and (e) H_2-reduced $Ce_{0.90}Ru_{0.10}O_{1.94}$.

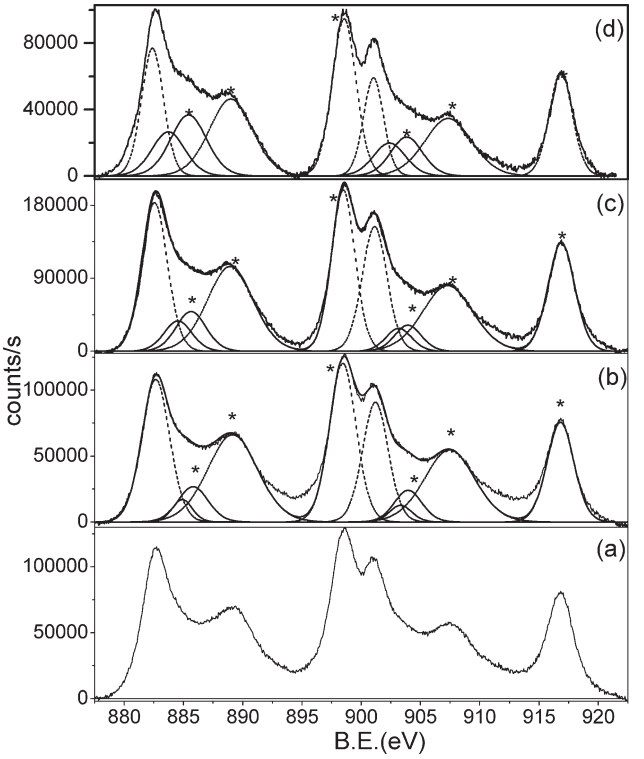

Figure 6. Ce (3d) core level XPS of a pure CeO_2, (b) as-prepared $Ce_{0.90}Ru_{0.10}O_{2-\delta}$, and (c) H_2 reduced $Ce_{0.90}Ru_{0.10}O_{2-\delta}$. (—) denotes Ce^{4+} peaks, (· · · · · ·) denotes Ce^{3+} peaks, and (*) denotes corresponding satellites peaks.

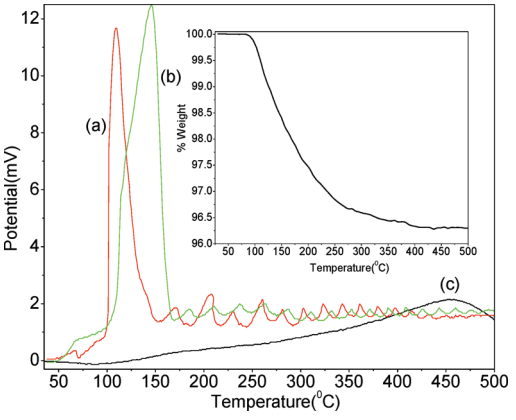

Figure 7. Hydrogen uptake plot for (a) $Ce_{0.95}Ru_{0.05}O_{1.94}$, (b) $Ce_{0.90}Ru_{0.10}O_{1.94}$, and (c) CeO_2. Inset, TGA curve for $Ce_{0.90}Ru_{0.10}O_{1.94}$ in hydrogen.

and $Ce_{0.90}Ru_{0.10}O_{1.94}$ for 5 and 10 at % Ru-ion-substituted CeO_2.

The presence of Ce^{3+} in $Ce_{1-x}Ru_xO_{2-x/2}$ can be explained from the redox potential of Ru^{3+}/Ru^{4+} (0.5 V)[33] and Ce^{IV}/Ce^{III} (1.61 V).[34] Accordingly, Ru^{3+} will get oxidized by Ce^{4+} in solution. In the synthesis of $Ce_{1-x}Ru_xO_{2-x/2}$, we have mixed Ce^{4+} and Ru^{3+} solution, leading to the redox reaction

$$Ce^{4+} + Ru^{3+} \rightarrow Ce^{3+} + Ru^{4+} \qquad (3)$$

So the formation of $Ce_{1-x}Ru_xO_{2-x/2}$ occurs via Ce^{4+} reduction followed by Ru^{3+} oxidation and it can be described as $Ce_{1-2x}{}^{4+}Ce_x{}^{3+}Ru_x{}^{4+}O_{2-x/2}$. Ionic radii of Ce^{4+} and Ce^{3+} in 8 coordination are 0.97 Å[35] and 1.23 Å,[35] respectively, and the ionic radius of Ru^{4+} in 6 coordination is 0.62 Å;[35] it should be have higher coordination in the fluorite lattice and have a higher ionic radius than 0.62 Å. Therefore, even though Ru^{4+} ion is smaller, because of Ce^{3+} ion and oxide ion vacancy, there is an increase in lattice parameter a of Ru-substituted CeO_2 (Table 1).

Oxygen storage capacity of $Ce_{1-x}Ru_xO_{2-x/2}$ is studied by hydrogen uptake measurements. H_2/TPR profile of $Ce_{1-x}Ru_xO_{2-x/2}$ ($x = 0.0.5$ and 0.10) and of CeO_2 up to 500 °C are shown in Figure 7. The H_2/TPR profile of CeO_2 made by melamine in similar condition is also shown in Figure 7 for comparison. The reduction temperature of $Ce_{1-x}Ru_xO_{2-x/2}$ is around 125 °C. From the amount of hydrogen taken up, $Ce_{0.95}Ru_{0.05}O_{1.97}$ reduced to $Ce_{0.95}Ru_{0.05}O_{1.75}$, which is equivalent to 0.22 mol of [O]/mol or 1334.8 μmol/g of [O]. $Ce_{0.90}Ru_{0.10}O_{1.94}$ is reduced to $Ce_{0.85}Ru_{0.15}O_{1.52}$, which is equivalent to 0.42 mol of [O]/mol or 2512.6 μmol/g of [O] up to 250 °C. The maximum oxygen storage capacity expected for $Ce_{0.5}Zr_{0.5}O_2$ is 0.25 mol of [O]/mol or 1693 μM/g, and the experimentally observed value up to 600 °C for one of the best $Ce_{0.5}Zr_{0.5}O_2$ samples is 0.22 mol of [O]/mol or 1500 μM/g up to 600 °C.[36] Therefore,

(33) Huheey, J. E., Keiter, E. A., Keiter, R. L. Inorganic Chemistry, 4th ed.; Pearson Education: Delhi, India, 2004.
(34) Cotton, F. A.; Wilkinson, G. Advanced Inorganic Chemistry, 3rd ed.; Wiley Eastern: New Delhi, India, 1972.
(35) Shannon, R. D. *Acta Crystallogr., Sect. A* **1976**, *32*, 751.
(36) Nagai, Y.; Yamamoto, T.; Yoshida, S.; Nonaka, T.; Okamoto, T.; Suda, A.; Sugiura, M. *Catal. Today* **2002**, *74*, 225.

Table 2. OSC Data for $Ce_{1-x}Ru_xO_{2-x/2}$ up to 500 °C

compd	composition before reduction	composition after reduction	oxygen storage capacity (OSC) (μmol/g)
CeO_2	$Ce^{4+}O_2$	$Ce_{0.84}^{4+}Ce_{0.16}^{3+}O_{1.92}$	464.3
$Ce_{0.95}Ru_{0.05}O_{1.97}$	$Ce_{0.89}^{4+}Ce_{0.06}^{3+}Ru_{0.05}^{4+}O_{1.97}$	$Ce_{0.71}^{4+}Ce_{0.24}^{3+}Ru_{0.05}^{0}O_{1.75}$	1334.8
$Ce_{0.90}Ru_{0.10}O_{1.94}$	$Ce_{0.78}^{4+}Ce_{0.12}^{3+}Ru_{0.10}^{4+}O_{1.94}$	$Ce_{0.32}^{4+}Ce_{0.54}^{3+}Ru_{0.10}^{0}O_{1.52}$	2512.6

$Ce_{1-x}Ru_xO_{2-x/2}$ ($x = 0.05$ and 0.10) show very high OSC at much lower temperature compared to $Ce_{0.5}Zr_{0.5}O_2$. Such a high OSC of $Ce_{0.90}Ru_{0.10}O_{1.94}$ is also confirmed by thermogravimetic (TG) study of $Ce_{0.90}Ru_{0.10}O_{1.94}$ in hydrogen. A TG reduction plot of $Ce_{0.90}Ru_{0.10}O_{1.94}$ in 10%H_2/Ar up to 500 °C is shown in inset of figure 7. Final composition of $Ce_{0.90}Ru_{0.10}O_{1.94}$ after H_2 reduction by TG study is found to be $Ce_{0.90}Ru_{0.10}O_{1.54}$, which is close to the value obtained from hydrogen uptake study. OSC data by hydrogen uptake measurement are summarized in Table 2. The H/Ru ratio is found to be as high as 8.8 in $Ce_{0.95}Ru_{0.05}O_{1.97}$ and $Ce_{0.90}Ru_{0.10}O_{1.94}$ compared to ideal H/Ru ratio (=4) for RuO_2. This is because Ru^{4+} is entirely reduced to Ru^0 (metal) in addition to partial reduction of Ce^{4+} to Ce^{3+}. Thus in $Ce_{1-x}Ru_xO_{2-x/2}$ not only entire Ru^{4+} can be reduced to Ru^0, it also promotes Ce^{4+} reduction to Ce^{3+}. Hydrogen uptake measurements were performed repeatedly by reducing in H_2 up to 500 °C and oxidizing it in O_2 at 250 °C as shown in Figure 8 and it is fully reversible. Powder XPD pattern of $Ce_{0.90}Ru_{0.10}O_{1.95}$ reduced in H_2 up to 500 °C is given in Figure 1e. No impurity peaks corresponding to Ru metal or RuO_2 is observed. Rietveld refined powder XRD pattern of $Ce_{0.90}Ru_{0.10}O_{1.95}$ reduced in H_2 up to 500 °C viz, $Ce_{0.90}Ru_{0.10}O_{1.52}$ is also given in Figure 2(c). Lattice parameter, a of $Ce_{0.90}Ru_{0.10}O_{1.52}$ is further increased to higher value ($a = 5.4154(1)$ Å) compared to as prepared $Ce_{0.90}Ru_{0.10}O_{1.95}$ ($a = 5.4149(2)$ Å). Structural parameter of reduced sample is summarized in Table1. Interestingly Ru metal is not separated out after hydrogen reduction and redox characteristic is repeatedly reproduced. This is possible because of redox potentials of Ru^{3+}/Ru^0 (0.60 V) and Ru^{4+}/Ru^{3+} (0.5 V) compared to Ce^{4+}/Ce^{3+} (1.61 V).[33,34] Thus reoxidation of Ru^0 occur as follows

$$3Ce^{4+} + Ru^0 \rightarrow 3Ce^{3+} + Ru^{3+} \quad (4)$$

and

$$Ce^{4+} + Ru^{3+} \rightarrow Ce^{3+} + Ru^{4+} \quad (5)$$

and Ce^{3+} will get oxidized in presence of O_2. Oxidation states of $Ce_{0.90}Ru_{0.10}O_{1.52}$ reduced in hydrogen up to 500 °C is also examined by XPS. Core level Ru(3d) and Ru(3p) of $Ce_{0.90}Ru_{0.10}O_{1.52}$ is given in Figures 4e and 5e, respectively. The Ru($3d_{5/2}$) peak is observed at 280.7 eV and the Ru($3p_{3/2}$) peak is observed at 462.2 eV, which is higher than the corresponding value of Ru(3d) at 280.1 eV and Ru(3p) at 461.1 eV in Ru metal but lower than the corresponding Ru(3d) and Ru(3p) states for Ru^{4+} in RuO_2. CeO_2 being insulating, a slightly higher

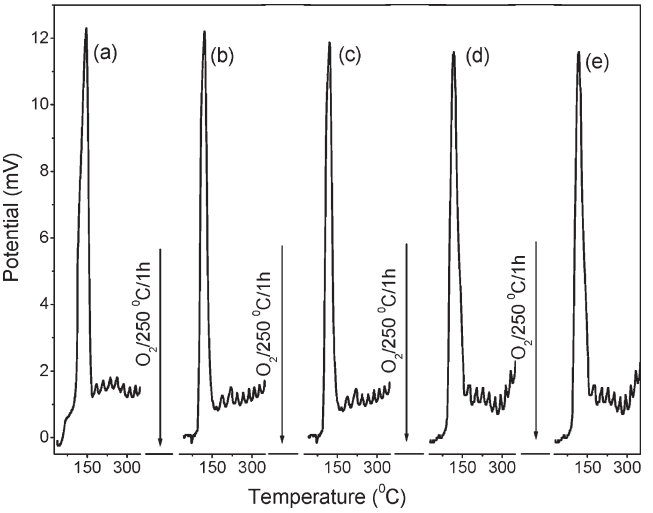

Figure 8. Hydrogen uptake plot of $Ce_{0.90}Ru_{0.10}O_{1.94}$ for five cycles (a−e) by reducing 5%H_2/Ar and reoxidising in pure O_2 at 250 °C.

binding energy for Ru^0 in CeO_2 is expected. So Ru is in zero-valence states in the hydrogen-reduced sample. XPS spectra of Ce(3d) in $Ce_{0.90}Ru_{0.10}O_{1.52}$ is shown in Figure 6d and ~45% of Ce is found in 3+ state and rest is in 4+ state. % Ce^{3+} values observed from XPS study in $Ce_{0.90}Ru_{0.10}O_{1.94}$ reduced in hydrogen up to 500 °C is close to the value calculated from OSC data. So XPS study also confirms the OSC result. Redox potential is playing a crucial role in reversible OSC property of $Ce_{1-x}Ru_xO_{2-\delta}$. A similar role of redox potential is also observed in reversible OSC of $Ce_{2/3}Cr_{1/3}O_{2+y}$ where oxidation of Cr^{3+} to Cr^{4+} and $Cr^{6+}$is occurred via Ce^{4+} to Ce^{3+} reduction.[13]

Having studied the OSC and reversible redox characteristic of these materials by H_2/TPR, compounds have been tested for CO oxidation, hydrocarbon oxidation and NO reduction by CO. Direct utilization of higher OSC or utilization of lattice oxygen of this material is also studied by CO oxidation in absence of feed oxygen. % CO conversions over $Ce_{0.95}Ru_{0.05}O_{1.97}$ and $Ce_{0.90}Ru_{0.10}O_{1.94}$ both in presence and in absence of feed oxygen are given in Figure 9. Complete conversion of CO to CO_2 is achieved below 105 °C with $Ce_{0.90}Ru_{0.10}O_{1.95}$ and below 135 °C with $Ce_{0.95}Ru_{0.05}O_{1.975}$ catalyst in presence of feed oxygen. Utilization of lattice oxygen is also shown with both catalysts when CO oxidation experiments are done in the absence of feed oxygen with the same space velocity. A higher percentage of CO conversion in the absence of feed oxygen suggests that lattice oxygen is activated by Ru ion substitution in ceria and tha tfeed O_2 can be reversibly exchanged with lattice oxygen, resulting in lower-temperature CO oxidation. Activation energies for CO oxidation with these catalysts

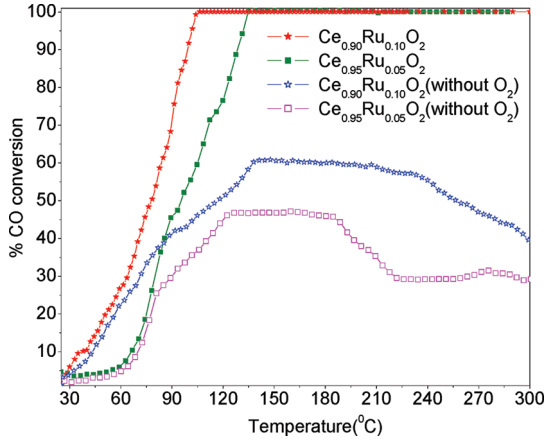

Figure 9. % CO oxidation with $Ce_{0.95}Ru_{0.05}O_{1.97}$ and $Ce_{0.90}Ru_{0.10}O_{1.94}$.

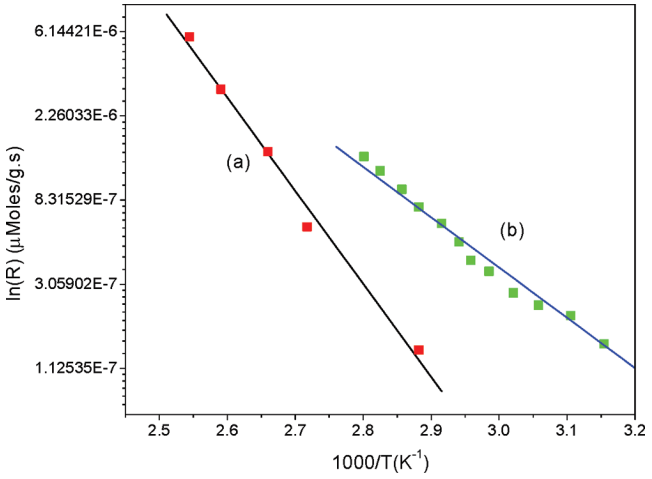

Figure 10. Ln(R) vs 1000/T Plot for CO oxidation with (a) $Ce_{0.95}Ru_{0.05}O_{1.97}$ and (b) $Ce_{0.90}Ru_{0.10}O_{1.94}$.

have been obtained at $<20\%$ conversion, and the rate of the reaction vs temperature for co-oxidation with $Ce_{0.95}Ru_{0.05}O_{1.97}$ and $Ce_{0.90}Ru_{0.10}O_{1.94}$ is given in panels a and b in Figure 10. Activation energies for CO oxidation with $Ce_{0.95}Ru_{0.05}O_{1.97}$ and $Ce_{0.90}Ru_{0.10}O_{1.94}$ are 92.2 and 43 kJ/mol, respectively. CO oxidation was also carried out with a 1:1 vol % CO:O_2 ratio with different weights of the catalysts to obtain the actual rates from the equation

$$\text{rate}(r) = (F/W)x \qquad (6)$$

where F is flow of gaseous molecules in mol/s, W is ; weight of the catalyst, and x is fractional conversion. Fractional conversion with W/F was plotted at different temperatures as shown in panels a and b in Figure 11 for $Ce_{0.95}Ru_{0.05}O_{1.97}$ and $Ce_{0.90}Ru_{0.10}O_{1.94}$ respectively. The weights of the catalysts, W, were varied from 25 to 100 mg, whereas F, the flow rate (mol/s), was kept constant. The plot is linear up to nearly 65% conversion, and the reaction rates at different temperatures were determined from the slopes of the linear region, shown in Figure 12. Activation energies were also calculated from rates derived from W/F plots. Activation energies for CO oxidation with $Ce_{0.95}Ru_{0.05}O_{1.97}$ and $Ce_{0.90}Ru_{0.10}O_{1.94}$ are 94.5 and 44.8 kJ/mol, respectively, which are closer to the

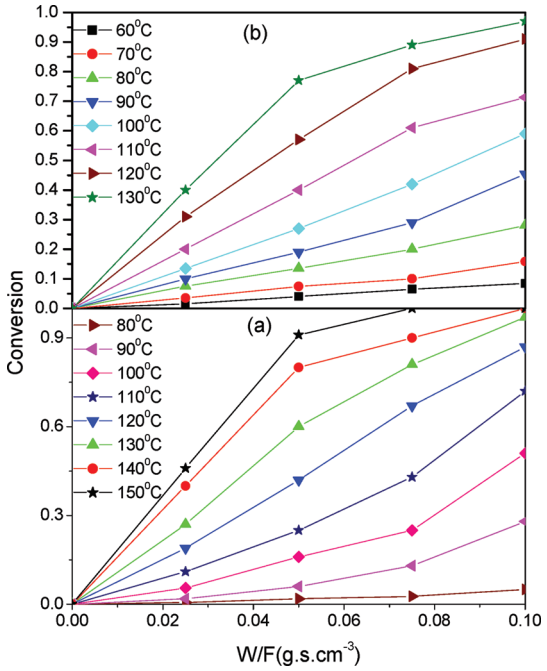

Figure 11. Fractional CO conversion vs W/F plot for (a) $Ce_{0.95}Ru_{0.05}O_{1.97}$ and (b) $Ce_{0.90}Ru_{0.10}O_{1.94}$.

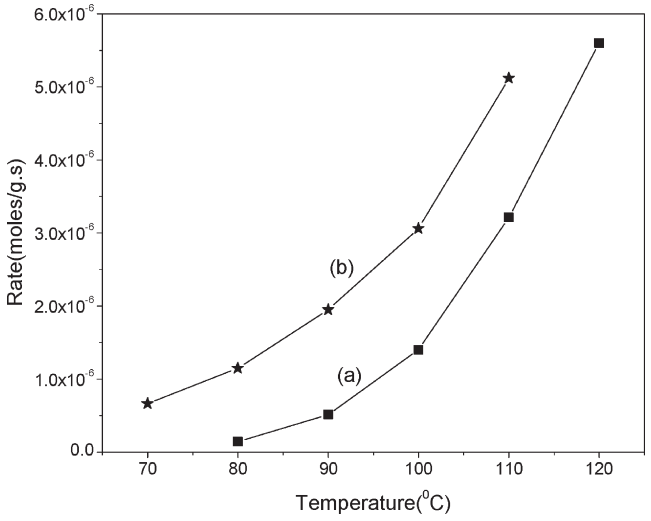

Figure 12. Rate vs temperature plot derived from conversion vs W/F plot for (a) $Ce_{0.95}Ru_{0.05}O_{1.97}$ and (b) $Ce_{0.90}Ru_{0.10}O_{1.94}$.

values obtained from the direct conversion plot with 200 mg of these catalysts. A comparison of rate and activation energy with different catalysts for CO oxidation is given Table 3. Both $Ce_{0.95}Ru_{0.05}O_{1.97}$ and $Ce_{0.90}Ru_{0.10}O_{1.94}$ are found to be superior to other noble-metal-ion-substituted and metal-impregnated catalysts.[16,21]

Hydrocarbon oxidation have also been studied over the catalysts and is shown in panels a and b in Figure 13. Complete oxidation of HC oxidation is achieved below 240 °C with the $Ce_{0.90}Ru_{0.10}O_{1.93}$ catalyst and below 280 °C with the $Ce_{0.95}Ru_{0.05}O_{1.97}$ catalyst. Complete oxidation of ethylene, acetylene, and propene is achieved below 125 °C and propane completely oxidized at 240 °C over $Ce_{0.90}Ru_{0.10}O_{1.93}$ catalyst, whereas with $Ce_{0.95}Ru_{0.05}O_{1.97}$ catalyst, complete oxidation of ethylene and acetylene occurs at 125 °C and propene and

Table 3. Data of Rate and Activation Energy for CO Oxidation

reaction	catalyst	rate (μmol/(g s)) / temperature (°C)	E_a (kJ/mol)	ref
CO + O_2	5 wt % Ru/SiO_2	1.00 (110)	94	15
	5 wt % Pd/SiO_2	0.316 (143)	103	15
	5 wt % Pt/SiO_2	0.32 (115)	56	15
	$Ce_{0.98}Pd_{0.02}O_{1.98}$	3.9 (120) 0.569(100)	121	20
	$Ce_{0.95}Ru_{0.05}O_{1.97}$	2.05(100)	92.2	present study
	$Ce_{0.90}Ru_{0.10}O_{1.94}$	3.3(100)	43	present study

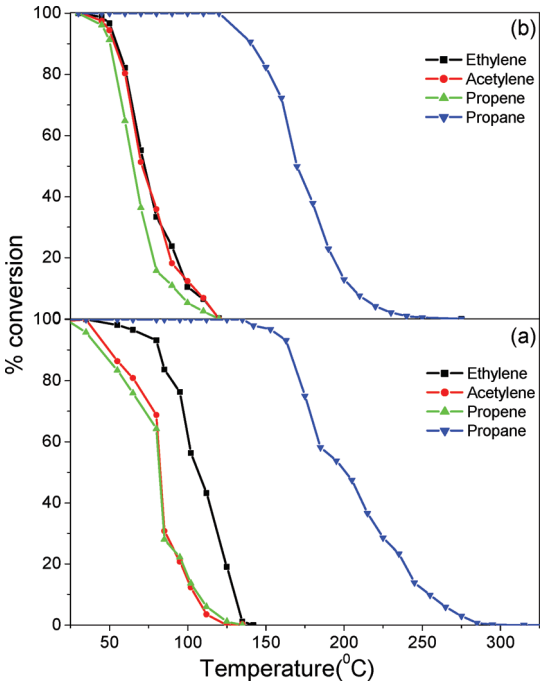

Figure 13. Hydrocarbon oxidation over (a) $Ce_{0.95}Ru_{0.05}O_{1.97}$, (b) $Ce_{0.90}Ru_{0.10}O_{1.94}$.

Table 4. Data of Rate and Activation Energy for Hydrocarbon Oxidation

reaction	vatalyst	E_a (KJ/ Mole)	rate (μmol/(g s)) (°C)
ethylene + O_2	$Ce_{0.95}Ru_{0.05}O_{1.97}$	62.6	0.143 (100)
	$Ce_{0.90}Ru_{0.10}O_{1.94}$	69.9	0.223 (100)
acatylene + O_2	$Ce_{0.95}Ru_{0.05}O_{1.97}$	72.1	0.227 (100)
	$Ce_{0.90}Ru_{0.10}O_{1.94}$	64.5	0.22 (100)
propene + O_2	$Ce_{0.95}Ru_{0.05}O_{1.97}$	78.3	0.123 (100)
	$Ce_{0.90}Ru_{0.10}O_{1.94}$	65.6	0.071 (100)
propane + O_2	$Ce_{0.95}Ru_{0.05}O_{1.97}$	128.2	0.074 (200)

propane completely oxidized at 140 and 280 °C, respectively. Activation energies and rates for HC (ethylene, acytelene, propene, and propane) oxidation with both $Ce_{0.95}Ru_{0.05}O_{1.97}$ and $Ce_{0.90}Ru_{0.10}O_{1.94}$ catalysts have been summarized in Table 4, and the rates of the reaction vs temperature for propane oxidation with $Ce_{0.95}Ru_{0.05}O_{1.97}$ and $Ce_{0.90}Ru_{0.10}O_{1.94}$ are given in Figure 14. For example, the activation energies for propane oxidation with $Ce_{0.95}Ru_{0.05}O_{1.97}$ and $Ce_{0.90}Ru_{0.10}O_{1.94}$ are 108.2 and 100.1 kJ/mol, respectively. Rates of hydrocarbon oxidation are also high with these catalysts; for propane oxidation, rates are 0.131 and 0.173 μmol/(g s) at 225 °C with $Ce_{0.95}Ru_{0.05}O_{1.97}$ and $Ce_{0.90}Ru_{0.10}O_{1.94}$, respectively. Activation energies for ethylene, acetylene, and propene are 62.6, 72.1, and 78.3

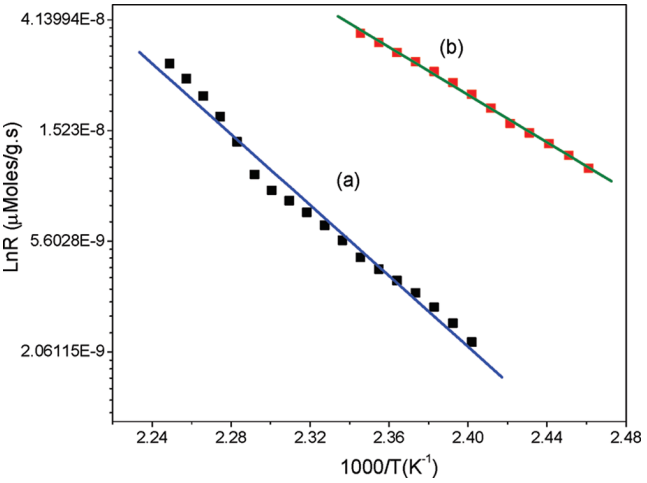

Figure 14. Ln(R) vs. 1000/T plot for propane oxidation with (a) $Ce_{0.95}Ru_{0.05}O_{1.975}$ and (b) $Ce_{0.90}Ru_{0.10}O_{1.95}$.

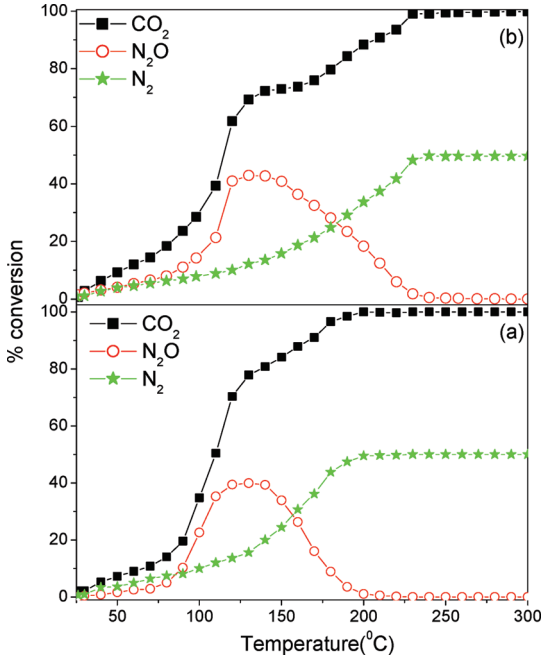

Figure 15. % NO reduction by CO with (a) $Ce_{0.95}Ru_{0.05}O_{1.975}$ and (b) $Ce_{0.90}Ru_{0.10}O_{1.95}$.

kJ/mol, respectively, for $Ce_{0.95}Ru_{0.05}O_{1.97}$ and 69.9, 64.5, and 65.6 kJ/mol for $Ce_{0.90}Ru_{0.10}O_{1.94}$.

Removal of NO_x (NO + NO_2) from exhaust stream of stationary and mobile sources has been a central challenge for environmental scientists.[37−39] The desired product from reduction of NO is N_2, but N_2O also forms, which is a powerful greenhouse gas that contributes to stratospheric ozone depletion.[39] NO reduction by CO with $Ce_{1-x}Ru_xO_{2-x/2}$ ($x = 0.05$ and 0.10) catalyst is shown in panels a and b in Figure 15. Complete conversion NO in to N_2 is observed at 200 °C with $Ce_{0.95}Ru_{0.05}O_{1.975}$ and at 250 °C with $Ce_{0.90}Ru_{0.10}O_{1.95}$, whereas at lower temperature, higher percentages of

(37) Hecker, W. C.; Bell, A. T. *J. Catal.* **1983**, *84*, 200.
(38) Oh, S. H.; Fisher, G. B.; Carpenter, J. E.; Goodman, D. W. *J. Catal.* **1986**, *100*, 360.
(39) Newton, M. A.; Jyoti, B.; Dent, A. J.; Fiddy, S. G.; Evans, J. *Chem. Comm.* **2004**, *21*, 2382.

Table 5. Data of Rate and Activation Energy for NO Reduction by CO

reaction	catalyst	rate (μmol/(g s)) /temperature (°C)	E_a(CO/CO_2) (kJ/mol)	% N_2 selectivity (°C)	ref
CO + NO	$Ce_{0.95}Ru_{0.05}O_{1.97}$	3.8 (200)	41	100 (200)	present study
	$Ce_{0.90}Ru_{0.10}O_{1.94}$	3.4 (200)	53.2	88 (200) 100 (240)	present study
	$Ce_{0.98}Pd_{0.02}O_{2-\delta}$	2.7 (250) 0.7 (200)	65	81 (200)	20

N_2O formation is observed. Generally NO reduction by CO occurs in two steps

$$\text{step I. } 2NO + CO \rightarrow N_2O + CO_2$$

$$\text{step II. } N_2O + CO \rightarrow N_2 + CO_2$$

$$\text{overall } 2NO + 2CO \rightarrow N_2 + 2CO_2$$

The noble metal ions are a potential adsorbent of NO and CO. This kind of adsorption will be mainly molecular adsorption, but NO can also get dissociatively adsorbed in the vacant site. Formation of N_2 as a product requires NO dissociation, whereas N_2O formation is the result of molecular NO adsorption.[40] It is expected that at lower temperature, NO and CO mainly get molecularly absorbed on largely available metal site. But as the reaction progresses, CO gets oxidized by lattice oxygen, creating more of an oxide ion vacancy; NO can get absorbed at the vacancy site, leading to dissociative chemisorptions. That is why $Ce_{1-x}Ru_xO_{2-x/2}$ shows low-temperature NO conversion to N_2 by CO and lattice oxygen activated by Ru substitution in ceria plays a key role in lower-temperature CO oxidation and NO reduction in to N_2 by CO. Activation energy of NO reduction or E_a(CO/CO_2) is found to be 41 kJ/mol for $Ce_{0.95}Ru_{0.05}O_{1.97}$ and 53.2 kJ/mol for $Ce_{0.90}Ru_{0.10}O_{1.94}$. Activation energy and rates with both $Ce_{0.95}Ru_{0.05}O_{1.97}$ and $Ce_{0.90}Ru_{0.10}O_{1.94}$ for NO_x reduction by CO are summarized in Table 5, and indeed, Ru-substituted CeO_2 is superior compared to other noble-metal-substituted CeO_2 and impregnated catalyst on support, both in terms of high rates and low activation energy.[20] As a whole, $Ce_{1-x}Ru_xO_{2-x/2}$ is not only shown to be higher OSC material than $Ce_{0.50}Zr_{0.50}O_2$ but because of the presence of Ru^{4+} ion and oxide ion vacancy, it acts as a catalyst by itself avoiding use of Pt, Pd metals. Both $Ce_{0.95}Ru_{0.05}O_{1.97}$ and $Ce_{0.90}Ru_{0.10}O_{1.94}$ have shown higher activity toward CO, "HC" oxidation, and NO reduction by CO in term of low activation energy and high rates of reaction.

(40) Granger, P.; Lecomte, J. J.; Dathy, C.; Leclercq, L.; Leclercq, G. *J. Catal.* **1998**, *175*, 194.

Conclusion

In summary, we have described the hydrothermal synthesis of $Ce_{1-x}Ru_xO_{2-x/2}$ ($x = 0.05$ and 0.10) using melamine as a complexing agent. $Ce_{1-x}Ru_xO_{2-x/2}$ crystallizes in the fluorite structure and $Ce_{0.90}Ru_{0.10}O_{1.94}$ shows much higher oxygen storage capacity than $Ce_{0.5}Zr_{0.50}O_2$. The role of redox properties of cerium and Ru is established in the formation $Ce_{1-x}Ru_xO_{2-x/2}$ phase and in its reversible OSC properties. Lattice oxygen is highly activated because of Ru substitution and it plays a key role in low-temperature CO, "HC" oxidation and complete conversion of NO in to N_2. Thus $Ce_{1-x}Ru_xO_{2-\delta}$ ($x = 0.05$, 0.10) acts as high OSC material as well as a uniform, solid three-way catalyst.

Acknowledgment. The authors thank the Department of Science and Technology, Government of India, for financial support. We thank Professor J. Gopalakrishnan for valuable discussion. Thanks are due to Amit Mondal and Sharad Kumar of Nano centre, Indian Institute of Science Bangalore, for recording TEM images.